RSC Advances

ROYAL SOCIETY OF CHEMISTRY

www.rsc.org/advances

Morphology evolution and impurity analysis of $LiFePO_4$ nanoparticles via solvothermal synthesis process

Xiankun Huang,[a] Xiangming He, *[a] Changyin Jiang[a] and Guangyu Tian[b]

[a] *Institute of Nuclear and New Energy Technology, Tsinghua University, Beijing 100084, PR China.*

[b] *State Key Laboratory of Automotive Safety and Energy, Tsinghua University, Beijing 100084, PR China*

**Corresponding Author: Fax: 86 10 89796031; Tel: 86 10 89796073; E-mail: hexm@tsinghua.edu.cn*

Abstract

A solvothermal method is applied for synthesizing $LiFePO_4$ nanoparticles using ethylene glycol as solvent. Crystals are obtained with quite different morphologies at various acidity solutions prepared via changing primary $LiOH/H_3PO_4$ mole ratios. SEM, TEM, HRTEM are used to analyze the samples. Element distribution in solid $LiFePO_4$ particles, mother solutions and washing solutions are tracked by ICP-OES and pH tests. Morphological test results show that the main exposed faces of samples transform from (100) as a rectangular shape to (010) as a spindle shape with pH of mother solutions increasing. Samples with predominant (010) face are formed at less acidic solvothermal solutions. At the intermediate pH from 3.11 to 3.73, powders like long hexagon nanorods are synthesized with (100) and (010) faces exposed. XRD results show that the long hexagon nanorods have better crystal structures synthesized at $LiOH/H_3PO_4$=2.7~3.0. Impurities like Fe_3O_4, Li_3PO_4, etc. are detected in spindle shape $LiFePO_4$ powders. The amount of impurities is related to the synthesis process and increases with the pH of solvothermal solution increasing. High temperature treatment is useful for impurities transforming to $LiFePO_4$ and thus reduces the impurities. The long hexagon nanorods show better electrochemical performances: 169.9mAh g-1 at 0.1C, and 129.8 mAh g-1 at 10C.

1. Introduction

Lithium iron phosphate ($LiFePO_4$) is one of the most promising cathode materials for lithium ion batteries for

its high electrochemical performances, low cost and good stability[1-6]. However, compared with layered lithium transition metal oxides ($LiMO_2$ (M=Co, Mn, Ni)) and spinel lithium manganese oxide ($LiMn_2O_4$), $LiFePO_4$ has a rather low electron conductivity and lithium ion diffusion constant because of its one-dimensional lithium ion transfer channel[7-9]. Therefore, efforts like carbon coating[10-12], supervalent doping[6, 13-15], nano-size and morphology tailoring[16-20] have been applied for solving this problem. Solvothermal (including hydrothermal) process has been researched a lot as an effective method to produce $LiFePO_4$ crystals which occurs in a lower temperature, cheaper and softer chemistry environment compared with solid state synthesis[21]. Synthesis procedure[22], solvent[23, 24], reaction temperature[25], reaction time[26], raw material ratio[27-30], pH of the reaction solution[31-34], reactant concentration[35, 36] and source[37] are important in determining crystal habit, crystal composition, crystal nucleation and growth rate during solvothermal process. Ethylene glycol (EG) has been proved as an optimal solvent for solvothermal synthesizing nano size $LiFePO_4$ particles with lower defect concentration[28, 38].

Nevertheless, during solvothermal process elements like Li, Fe and P et al. distributes in mother solutions, washing solutions and solid products which is different from that by solid state synthesis method. It is difficult for researchers to control element compositions of lithium iron phosphate by alternating Li, Fe and P ratios in precursors[39-41]. Composition range is small for nonstoichiometric lithium iron phosphate to stay as a homogeneous solid solution at ambient temperature. Phase separation and impurities' formation usually occur as Li:Fe:P deviates from 1:1:1[20, 42-44].Till now, there is no report on element distributions in solid phase products, mother solutions and washing solutions during solvothermal synthesis $LiFePO_4$ process. Reports on element distributions are mostly about element ratios of $LiFePO_4$ solid particles for those via hydrothermal methods[32, 45-49] and solvothermal process[29]. Systemically investigations of element behaviour are essential for better understanding of reaction mechanisms and influence parameters of solvothermal synthesis $LiFePO_4$.

This paper reported several $LiFePO_4$ particles with different morphologies synthesized at different acidity (pH) solutions using EG as solvent. Element distributions were analyzed in solid products, mother solutions and washing solutions during the whole process. It's worth to mention that the orientation of $LiFePO_4$ particles changes from (100) to (010) as pH of mother solution increases from 2.56 to 5.80. The impurities also increased as pH increases. The impurity formation process was illustrated in details. High temperature treatment is useful

not only for defect elimination but for impurity abatement.

2. Experimental

2.1 Synthesis

All the chemicals (AR grade) were purchased from Xilong Chemical Co., Ltd. Several samples were prepared by a solvothermal method using EG as solvent. The synthesis of $LiFePO_4$ was carried out in a 50ml Teflon vessel, which was sealed in a stainless-steel autoclave. $LiOH{\cdot}H_2O$, $FeSO_4{\cdot}7H_2O$ and H_3PO_4 (85 wt%) were chosen as Li, Fe, P sources. 7mmol $FeSO_4{\cdot}7H_2O$ was used in this process (which was set as 1in the following table 1). The amount of $LiOH{\cdot}H_2O$ and H_3PO_4 was added just as calculated by Li:Fe:P mole ratio. The typical feeding sequence was chosen: (P→Fe)→Li. H_3PO_4 was mixed with $FeSO_4$'s EG solution firstly and then this mixture was dripped into LiOH's EG solution to make green black slurry. Then the slurry was transferred into a Teflon vessel. The prepared Teflon vessel was then heated at 180℃ for 10h. After the solvothermal reactions finished, the supernatants were collected and diluted to one fifth with deionized water and the acidity (pH) of the solutions were measured. pH results in our work were all tested by this method. The obtained precipitates were washed with deionized water and ethanol for several times and then dried at 60℃ for over 6h. In order to obtain carbon-coated $LiFePO_4$/C powder with good electronic conductivity, the samples were mixed with 10wt% sucrose and sintered at 650˚C for 5h under argon atmosphere. The product $LiFePO_4$/C powder has a ~4% carbon content.

Table 1 Samples synthesized at different $LiOH/H_3PO_4$ mole ratios.

Sample	Li:Fe:P(mole ratio)	$LiOH/H_3PO_4$	shape
S1	2.7:1:1.5	1.8	rectangular nanoplate
S2	2.4:1:1	2.4	rectangular nanoplate
S3	2.7:1:1	2.7	long hexagon nanorod
S4	3.0:1:1	3.0	long hexagon nanorod
S5	3.1:1:1	3.1	spindle plate
S6	3.15:1:1	3.15	spindle plate

2.2 Characterization

The morphologies of the samples were observed using scanning electronic spectroscopy (SEM, JSM-5600LV, JEOL, Japan) at 20.0kV. Transmission electron microscope (TEM) imaging was performed using a JEM-2011

electron microscope operated at 200 kV. The X-ray diffraction(XRD) patterns of samples were recorded on a Rigaku D/Max 2500 diffractometer operated at 40 kV voltage and a 200 mA current with Cu Kα radiation (λ=1.5418Å). The inductively coupled plasma optical emission spectrometry (ICP-OES) of samples was performed on n IRIS Intrepid II XSP (Thermo Fisher). Working parameters: RF Power: 1150W, Nebulizer Flow: 26.0 PSI, Auxiliary gas: 1.0 LPM. The pH values of the supernatants were measured by a microprocessor pH meter (PHS-25, Shanghai).

2.3 Electrochemical measurements

The electrochemical performances were measured by using a 2032-type coin cell. The electrode was prepared by mixing a mixture of active materials, conductive graphite, acetylene black, and polytetrafluoroethene (PTFE) binder in a mass ratio of 6:2:1:1. Pure metallic lithium was used as anode. The electrolyte was 1M LiPF6 dissolved in volume ratio of 1:1:1 with ethylene carbonate/dimethyl carbonate/ethylmethyl carbonate. The cells were assembled in an argon-filled glove box. Galvanostatical charging–discharging tests were carried out on a Land CT2001A cycler (Wuhan Kingnuo Electronic Co.) in a voltage range 2.5–4.2V.

3. Results and discussion

3.1 Morphology evolution and crystal structure analysis

The $LiFePO_4$ powders were prepared via a solvothermal synthesis process by changing primary $LiOH/H_3PO_4$ mole ratio (i.e., changing reaction acidity). Fig.1 shows the shape and size of the $LiFePO_4$ samples obtained by SEM. It shows well dispersed and uniform particles in Fig. 1. From Fig. 1(a) and (b), we can get that S1and S2 particles are rectangular nanoplates with a large surface of 150nm×250nm and thickness of 25nm. There are few differences between S1 and S2. The samples S3 and S4 show quite different morphologies, which are about 40nm×50nm×90nm and 40nm×60nm×110nm nanorods with a large surface like long hexagon or rectangular. S4 nanorods have almost the same morphology with S3. While compared with S1~S4 nanoparticles, S5 and S6 crystals show larger sizes and a spindle like plate shape. The spindle plate grows larger when we increased the $LiOH/H_3PO_4$ mole ratio from 3.1 to 3.15. The width increased from 150nm to 190nm; the length increased from 300nm to 350nm; and the thickness increased from 60nm to 80nm. Orientation is an important parameter for

$LiFePO_4$ as we discussed for its one dimensional lithium ion channel. We have done TEM examinations to determine the main exposed facets of these crystals with different morphologies shown in Fig. 2. Fig. 2(a) shows sample S1's rectangular surface details. According to its corresponding fast Fourier transformation (FFT) image and lattice distances, the S1 sample has predominantly (100) face exposed. In Fig. 1(c) and (d) there are two kinds of facets exposed of S3: rectangular and long hexagon. Fig. 2(b-1) shows the details of long hexagon faces. As marked in Fig. 2(b-1)(middle and right), this face is determined as (010) face. While the rectangular face in Fig. 2(b-2) is shown the same (100) face. It can be determined that there is a thin amorphous layer on the surface of the sample. For sample S5, the exposed main surface is the spindle (010) face as shown in Fig. 2(c). There are small particles on the surface of the big spindle crystal, which can also be observed in Fig. 1(e) and (f). Results in Fig.1 and 2 show that the predominantly exposed faces of samples S1~S6 transform (100) faces to (010) faces as $LiOH/H_3PO_4$ increases from 1.8 to 3.15.

The thickness of crystals along [010] direction is detected using X-ray powder line-profile fitting based on the Scherrer function by scanning the (211/020) peak of 2θ range 28.5~31.0° (details are shown in supporting information part 2)[50-53]. The results data for the six samples are 62.5nm, 51.1nm, 29.0nm, 36.9nm, 30.0nm, 34.3nm for S1~S6 individually which is different from those observed by SEM and TEM (150nm, 150nm, 40nm, 50nm, 80nm, 80nm for S1~S6). According to the measurement principles of XRD, the thickness of [010] direction is in fact the coherence length along [010] direction. The reasons for the differences might be defects or crystal distortions in $LiFePO_4$ crystals[54]. Fig. 3 shows the X-ray diffraction pattern of samples S1-6 observed from solvothermal synthesis. All of them can be indexed to the standard pattern of orthorhombic olivine type $LiFePO_4$ (space group Pnma, JCPDS Card No. 83-2092). While for samples S5 and S6 with $LiOH/H_3PO_4$=3.1 and 3.15 (mole ratio) individually, the impurity iron diiorn(III) oxide Fe_3O_4(space group Fd-3m, JCPDS Card No. 227) is also indexed beside $LiFePO_4$ phase over 2θ range 60.9° to 63°. This impurity might refer to the small particles on the surface of the spindle plate shape crystals S5 and S6. For samples S1~S4 there are no evident impurities detected before the high temperature carbon coating. The detailed discussions about impurities are shown later.

The crystal parameter changes with $LiOH/H_3PO_4$ mole ratio are also tracked by doing Rietveld refinements on XRD patterns of S1~S6 $LiFePO_4$ samples, shown in table 2. Before carbon coated, the cell parameters a, b

and cell volume V climb up and then decline with $LiOH/H_3PO_4$ increasing from 1.8 to 3.15, while c increases first then decreases. S3 and S4 with $LiOH/H_3PO_4$ mole ratio 2.7 and 3.0 crystallized the best before high temperature treatment. When samples are carbon coated at high temperature in Ar atmosphere, cell parameters a, b and V increase a lot and c decreases. The cell volumes of all samples have increased after high temperature carbon coated for better crystallization. The cell volume differences between samples before and after high temperature carbon coated are quite different. The value of that is smaller for samples S3 and S4 with $LiOH/H_3PO_4$ mole ratio 2.7 and 3.0.

Table 2 Lattice parameters a, b, c and V(cell volume) of $LiFePO_4$ particles with and without carbon coated prepared at different $LiOH/H_3PO_4$ mole ratios. The Δ_V shows the smallest value of samples S3 and S4.

Samples	without carbon coated				with carbon coated				Δ_V[a]
	a	b	c	V	a	b	c	V	
S1	10.3000	5.9859	4.6963	289.5498	10.3155	5.9986	4.6916	290.3095	0.76
S2	10.3016	5.9865	4.6973	289.6849	10.3108	5.9964	4.6943	290.2391	0.55
S3	10.3071	5.9918	4.6982	290.1524	10.3121	5.9999	4.6929	290.3574	0.20
S4	10.3064	5.9953	4.6949	290.1012	10.3131	6.0032	4.6909	290.4234	0.32
S5	10.3029	5.9848	4.7014	289.8946	10.3211	6.0014	4.6932	290.7008	0.81
S6	10.3011	5.9812	4.7012	289.6579	10.3243	6.0029	4.6966	291.0757	1.42

a. Δ_V is the cell volume difference between cells with and without carbon coated.

There are free ions like H^+, $H_xPO_4^{x-3}$,$FeH_yPO_4^{y-1}$, Fe^{2+}, $Fe(OH)_z^{2-z}$, etc. and complexes like Fe^{2+}-EG, Fe^{2+}-SO_4^{2-}, $LiFePO_4$ crystal surface-EG, $LiFePO_4$ surface- SO_4^{2-}, etc in the solvothermal reaction system. It has been approved the $LiFePO_4$ solvothermal (including hydrothermal) process is a dissolution-recrystallization process[26]. The upper free ions and complexes' concentration will have a big influence on $LiFePO_4$ crystal growth. However, the free ions' concentration and complexes' concentration are decided by solution acidity (pH) of the whole solvothermal process. Meanwhile, the precipitates like Li_3PO_4, $Fe_3(PO_4)_2$, and $Fe(OH)_2$'s dissolution process are also influenced by solution acidity(pH). Therefore, solution acidity (pH) is an important parameter that influences the whole $LiFePO_4$ solvothermal process. Here we can find the influences on $LiFePO_4$ crystal habit on Fig. 1 and 2. We tested the acidity (pH) of the supernatant of samples S1~S6 via solvothermal process by changing with $LiOH/H_3PO_4$ mole ratio. The results are 2.59, 2.78, 3.11, 3.73, 5.80, 6.55 for S1~S6 individually. The predominantly exposed faces of $LiFePO_4$ samples change from (100) face to (010) face with the solution acidity decreased (pH increased) shown in Fig. 4. To confirm the acidity (pH) influences on the morphology revolution, further experiments are done as that Li_2SO_4 is used as part of Li resource instead of

LiOH for preparing $LiFePO_4$ particles. We use 2.7:0.25:1:1 (2.7-LiOH, 0.25-Li_2SO_4, 1-$FeSO_4$, and 1-H_3PO_4) as reactants ratio and get almost the same long hexagon nanorods as that by 2.7:1:1(2.7-LiOH) instead of spindle plates made by 3.2:1:1(3.2-LiOH). And we also checked the influence of feeding sequences of the Li, Fe and P resources on $LiFePO_4$ crystal morphology. Feeding sequence Fe→(P→Li) was applied to produce samples. H_3PO_4 was added to LiOH's solution first to form a white suspension, and then $FeSO_4$'s EG solution was dripped inside. Three samples with $LiOH/H_3PO_4$=1.8, 3.0 and 3.15 individually were produced. The morphology variation of samples (as shown in Fig. S1 and S2) was almost the same as that of samples made by (P→Fe)→Li. As reported by Wang's work[55], surface (100), (010) and (101) are lowest energy faces which prefer to be kept during $LiFePO_4$ crystal process. And naked faces like (100) and (010) faces include a lot of unsaturated coordinated Li and Fe and naked O. Then these naked faces will absorb H^+, SO_4^{2-}, Fe^{2+}, OH^-, EG, $HO\text{-}CH_2\text{-}CH_2\text{-}O^-$ or $^-O\text{-}CH_2\text{-}CH_2\text{-}O^-$, etc. to stabilize themselves. For the surface energy is changed by the absorption behaviour. Therefore the crystal habit is changed. There is an isoelectric point of $LiFePO_4$ particle in EG solvent which is always described as a pH value. Here we set the isoelectric point as *i*. When the solution pH<*i*, the net residual electric charge on the surface of the $LiFePO_4$ particles is expected to be positive, thus the absorption of cations is weakened. Faces are covered by different kinds of OH^-, SO_4^{2-}, $HO\text{-}CH_2\text{-}CH_2\text{-}O^-$ or $^-O\text{-}CH_2\text{-}CH_2\text{-}O^-$ ions and complexes selectively. While when pH>*i*, the particle surface is negatively charged. Particle surfaces will be capped by EG molecules. As reported by first principle calculations and hydrothermal experiments[56, 57], water-capped $LiFePO_4$ particles favour to form exposed (010) face. It is reasonable to hypothesis that EG-covered $LiFePO_4$ crystals have the (010) predominantly exposed face. High pH value creates a high supersaturating level which results in a fast nucleation process generating precursor precipitates. The saturated precursor is difficult to dissolution at higher pH value. The $LiFePO_4$ crystal growth kinetics is controlled by diffusion and surface reaction for this dissolution-recrystallization process. Thus the growth kinetics of $LiFePO_4$ crystals are controlled by dissolution process of precursors which resulted in larger crystal size. The whole process is schemed in Fig. 5.

3.2 Electrochemical performances

Because of the $LiFePO_4$ growth in a preferred orientation for lithium ion transferring, it is reasonable for us to

hypothesis the samples S3, S4, S5 and S6 will get excellent electrochemical performances. However, this is not the case. The electrochemical performances of the six carbon coated samples are shown in Fig. 6. S3 and S4 show the best power performances: with S3, the battery has a 131.3 mAh g^{-1} specific discharge capacity and that with S4 has a 129.8 mAh g^{-1} specific discharge capacity at 10C. The S5 and S6 samples which should have got better performances, have got as worst as about 70mAh g^{-1} discharge capacity at 0.1C and 15mAh g^{-1} at 10C. S1 and S2 has a less discharge capacity of 84 and 118.1 mAh g^{-1} at 10C compared with S3 and S4. This is due to the larger crystal sizes along b axis for about 60 and 50 nm of S1 and S2 compared with about 40nm for S3 and S4. The discharge performance of S4 varies with discharge current increasing from 0.1C to 10C as shown in Fig. 7. It has got a specific discharge capacity of 169.9, 155.8, 147.0, 145.5, 143.1, 138.5 and 129.8 mAh g^{-1} individually. The bad performances of S5 and S6 are might because of the bigger crystal particle sizes compared with S1~S4 and more impurities as detected by SEM, TEM and XRD. Although the calculated results of the length along b axis of S5 and S6 are small (about 30nm), while in Fig. 1 the SEM images shows about 60~80nm length along [010] direction. The big difference between these two data might refer to a large number of defects or crystal distortions[54]. In addition, impurity content is also an important parameter that influences the $LiFePO_4$ particles' performances.

3.3 Impurity analysis

As mentioned in section 1, compared with traditional solid-state synthesis $LiFePO_4$ method, liquid-phase method like hydrothermal or solvothermal way has a more complicated element distribution during the producing process. There are Li, Fe, P, S elements not only in solid products, the supernatant mother solutions, but in the washing solutions which are produced before clean $LiFePO_4$ samples are obtained. Thus it is very difficult to get stoichiometric $LiFePO_4$ samples which are critical for $LiFePO_4$ crystal structure and performances. To illustrate the element distribution map of solvothermal synthesis $LiFePO_4$ process, we tested the amount of Li, Fe, P, S elements in solid $LiFePO_4$ products, mother solutions and washing solutions as $LiOH/H_3PO_4$ mole ratio changes from 1.8 to 3.15. Table 3 shows the ICP-OES test results of Li, Fe, P, S amount in solid products and mother solutions. As it can be observed, (1) the amount of element Li, Fe, P, S in mother solutions decreases with $LiOH/H_3PO_4$ mole ratio increases. Almost all the Fe has been precipitated as

solid phase and there's little left in mother solutions. 74.5% Li_2SO_4 solute in mother solution at $LiOH/H_3PO_4$=1.8 of S1, while this value decreased to 35.8% at $LiOH/H_3PO_4$=2.7 of S3, and when $LiOH/H_3PO_4 \geq 3$, less than 20% Li_2SO_4 solute in mother solutions. (2) In solid phase products, Li/Fe>1, and P/Fe<1, compared with pure $LiFePO_4$ where Li:Fe:P=1:1:1, which means that there are impurities in the solid phase products. There is S element detected in solid products and the amount increases with $LiOH/H_3PO_4$ increases. Li_2SO_4, $FeSO_4$ or other insoluble impurities stay in solid products. P/Fe is less than1 in solid phase. So where is the other part of P? Take sample S3 as an example: P in solid phase is 93.4%, and 3.8% is in mother solution, the sum of P is 97.2%<1(as $Fe/Fe_0 \approx 1$, here we neglect the difference between Fe and Fe_0). The left 2.8% should be washed away. To get this part of P, we tested the amount of elements in washing solution. The data are shown in table 4. Neglect the loss of Fe during the washing process (0.13% is washed away). Combined table 3 and table 4, the material balance results of P is 1.003 with the error 0.3%.

Table 3. pH of mother solutions produced with various $LiOH/H_3PO_4$ and Li, Fe, P, S element amount in both solid phase products and mother solutions tested using ICP.

Sample	$LiOH/H_3PO_4$	pH[b]	solid phase (mole ratio)			mother solution (mole ratio)			
			Li/Fe	P/Fe	S/Fe	Fe/Fe_0	Li/Fe_0	P/Fe_0	S/Fe_0
S1	1.8	2.59	1.115	0.964	0.044	0.004	1.276	0.496	0.745
S2	2.4	2.78	1.094	0.911	0.073	0.0009	0.791	0.075	0.566
S3	2.7	3.11	1.161	0.934	0.071	0.0003	0.554	0.038	0.358
S4	3.0	3.73	1.264	0.963	0.082	0.0004	0.371	0.026	0.169
S5	3.1	5.80	1.303	0.887	0.170	0.0003	0.411	0.001	0.185
S6	3.15	6.55	1.350	0.887	0.171	0.0007	0.418	0.001	0.192

b. pH of Mother solutions.
Fe_0: initial $FeSO_4$ content (mol)

Table 4. Li, Fe, P, S amount in first 3 times' washing solutions during producing S3 process.

Washing solution(mole ratio)	Fe/Fe_0	Li/Fe_0	P/Fe_0	S/Fe_0
First 3 times	0.0013	1.134	0.031	0.554

In summary, there are a lot of impurities in samples made from solvothermal process at various $LiOH/H_3PO_4$ mole ratios, even there is no evident extra peaks in S1~S4 samples. The impurities is amorphous phase existed on the surface of $LiFePO_4$ crystal as shown in Fig. 2(b). High temperature treatment enables the amorphous impurities to crystallize. Fig. 8 shows the comparisons of S1, S3 and S5 treated at 650℃ for 5 hours with and without carbon coated under Argon atmosphere. There are crystallized Li_3PO_4 and Fe_3O_4 impurities in both S3-a and S5-a which are annealed without carbon coated and the later have stronger impurity peaks as shown in Fig.

8(a). However after carbon coating, there is no evident impurities on the XRD patterns of S3-c. This is might because of surface reaction of Li_3PO_4 and Fe_3O_4 which existed on the surface of S3 and S5. Sucrose and the subsequent pyrolytic carbon also hinder the nucleation and growth of impurities. The Fe_3O_4 peaks intensity of S5-c have an obvious decrease compared with that of S5-a. A new $Fe_3Fe_4(PO_4)_6$ peak appears on the XRD pattern of S5-c.

As we discussed in our previous paper, reactions occurred as follows during the whole solvothermal process:

$$3Fe^{2+} + 2{PO_4}^{3-} \leftrightarrow Fe_3(PO_4)_2(s) \quad (1)$$

$$3Li^{+} + {PO_4}^{3-} \leftrightarrow Li_3PO_4(s) \quad (2)$$

$$Fe^{2+} + H_2O \leftrightarrow Fe(OH)_2(s) + 2H^{+} \quad (3)$$

$$Li^{+} + Fe^{2+} + {PO_4}^{3-} \leftrightarrow LiFePO_4(s) \quad (4)$$

when H_3PO_4 and $FeSO_4$'s mixed EG solution dripped into LiOH's EG solution, phosphate ions react with ferrous ions or lithium ions to form precipitates $Fe_3(PO_4)_2$ or Li_3PO_4. Ferrous ions also participate in a hydrolysis reaction. Precipitates like $Fe_3(PO_4)_2$, Li_3PO_4, $Fe(OH)_2$ constitute the precursors which solutes gradually in the solvothermal reaction process and form $LiFePO_4$ crystal. The left $Fe_3(PO_4)_2$, Li_3PO_4, $Fe(OH)_2$ precursors and Li_2SO_4 or $FeSO_4$ which was not washed away are the main source of impurities of solid products produced via solvothermal method.

(1)$Fe(OH)_2$

If we set Li/Fe=a, P/Fe=b, and S/Fe=c, using element conservation method we can get that the content of $Fe(OH)_2$ in the solid products is only related to a, b and c. (Set the mole ratio of $LiFePO_4$, $Fe_3(PO_4)_2$, Li_3PO_4, Li_2SO_4, $FeSO_4$, and $Fe(OH)_2$ in solid products as x_1~x_6 respectively. From element conservation, functions $x_1+3x_3+2x_4=a$; $x_1+2x_2+x_3=b$; $x_1+3x_2+x_5+x_6=1$; $x_4+x_5=c$ are built. We can get $x_6=1+a/2-3b/2-c$.) Table 5 gives the results of contents of $Fe(OH)_2$ in the six samples. The content of $Fe(OH)_2$ increases as the original $LiOH/H_3PO_4$ increases. This is because that when $LiOH/H_3PO_4$ increases the acidity of the reaction solution decreases which enhances reaction (3) and decreases the solubility of $Fe(OH)_2$. There are more $Fe(OH)_2$ left in the result powders which converts to iron oxide (Fe_3O_4) after drying or annealing. The content of $Fe(OH)_2$ might

be decreased by reacting with Li_3PO_4 during high temperature annealing process. The reaction mechanism is shown as reaction (5).

$$Fe(OH)_2 + Li_3PO_4 \leftrightarrow LiFePO_4 + Li_2O + H_2O \quad (5)$$

Table 5 $Fe(OH)_2$ contents of solid samples synthesized at different $LiOH/H_3PO_4$ mole ratios.

Sample	S1	S2	S3	S4	S5	S6
$LiOH/H_3PO_4$ (mole ratio)	1.8	2.4	2.7	3.0	3.1	3.15
$Fe(OH)_2/Fe_0$(mole ratio)	0.069	0.108	0.109	0.106	0.151	0.174

(2) Li_3PO_4

Reaction (1) (3) and (4) are competitive reactions which all consume ferrous ions. The reaction degree of reaction (3) increases with $LiOH/H_3PO_4$ increasing, which inhibited the generation of $Fe_3(PO_4)_2$ in the beginning of solvothermal process so that more phosphate ions can involve into reaction (2) and generate more Li_3PO_4. $Fe(OH)_2$ will release free Fe^{2+} after $Fe_3(PO_4)_2$ exhausted during solvothermal process. As it's more difficult for $Fe(OH)_2$ dissociation especially at high pH, the left Li_3PO_4 content increases as $LiOH/H_3PO_4$ increases when the solvothermal process ends. This is in constant with that the solid phase Li/Fe ratio increases when $LiOH/H_3PO_4$ increases as shown in table 3. The left Li_3PO_4 content will be decreased through reaction with $Fe(OH)_2$ and $Fe_3(PO_4)_2$ on the $LiFePO_4$ particle surfaces during subsequent annealing process. The reaction of Li_3PO_4 and $Fe_3(PO_4)_2$ is shown as follows:

$$Fe_3(PO_4)_2 + Li_3PO_4 \leftrightarrow 3LiFePO_4 \quad (6)$$

(3) SO_4^{2-}

There is residual SO_4^{2-} in every $LiFePO_4$ samples which is usually washed for 3 times by water and once by ethanol. To check if this was due to inadequate wash, we have done a washing experiment by washing sample S3 for 20 times. Table 6 and 7 list out the content of Li, Fe, P, S elements in solid products and washing solutions tested by ICP-OES. From table 6 we can find that after 3 times wash, there are still 6~7%SO_4^{2-} in the samples. During the following 4~20 times' wash, the residual S changes little in solid products. Thus the S element might exist as insoluble impurities and it does not exclude the possibility that S enters into $LiFePO_4$ olivine lattice as a substitution at P site (partially replace of PO_4^{3-} by polyanoin SO_4^{2-}).

Table 6 Element contents of solid samples washed for different times

Solid phase(mole ratio)	Fe/Fe_0	Li/Fe_0	P/Fe_0	S/Fe_0
after 3^c+1^d	0.999	1.041	0.882	0.072
after 10^c+1^d	0.963	0.981	0.840	0.064
after 20^c+1^d	0.926	0.922	0.799	0.062

c. times washed by water.
d. times washed by ethanol.

Table 7 Element contents of washing solutions at different washing conditions

Washing solution(mole ratio)	Fe/Fe_0	Li/Fe_0	P/Fe_0	S/Fe_0
within first 3 times wash	0.0013	1.134	0.031	0.554
4^{th} to 10^{th} time wash	0.035	0.057	0.042	0.0034
11^{th} to 20^{th} time wash	0.037	0.060	0.044	0.0033

Table 6 shows a lot of Li_2SO_4 was washed during the first 3 times by water. The content of Fe is as low as 0.13%, and it is reasonable to assume the washed 3.1% P comes from impurities like Li_3PO_4 instead of product $LiFePO_4$. During the 4^{th} to 20^{th} washing process, the total amount of Li, Fe and P are 11.7%, 7.2% and 8.6% individually, which is further more than that of S (0.67%). The main phase $LiFePO_4$ might be washed out during the 4^{th} to 20^{th} washing process. It needs further research about the existing form of S.

4. Conclusion

Six $LiFePO_4$ particles with different sizes and shapes are synthesized at various $LiOH/H_3PO_4$ mole ratios prepared by solvothermal synthesis method using ethylene glycol as solvent. Obvious morphology evolution is obtained during $LiOH/H_3PO_4$ mole ratio increasing from 1.8 to 3.15. Rectangular nanoplate with the main face of (100) transform to spindle plate with the predominant face of (010), and the intermediate state is a long hexagon nanorod with large (010) face and (100) face. Electrochemical tests of these samples show that the $LiFePO_4$ performances are related to the crystal sizes, crystal thickness along b axis and impurities' contents.

By analyzing the ICP-OES results of $LiFePO_4$ solid products, mother solutions, and washing solutions, element distributions are described in detail. Results indicate that the formation of impurities of $Fe(OH)_2$ (Fe_3O_4) and Li_3PO_4 is promoted as $LiOH/H_3PO_4$ mole ratio increases. The impurities on the surface of the product $LiFePO_4$ particles can transform to $LiFePO_4$ during high temperature annealing process to a certain extent. Almost all $LiFePO_4$ samples synthesized by solvothermal process have S element in it which cannot be washed away thoroughly even for 20 times. Further researches are needed to identify the form of S element

existing in $LiFePO_4$ samples. It might exist as an insoluble impurity on the surface of $LiFePO_4$ or enter into the $LiFePO_4$ olivine lattice in solid solution.

Acknowledgements

This work is supported by the MOST (Grant No. 2013CB934000, No. 2011CB935902, No. 2014DFG71590, No. 2010DFA72760, No. 2011CB711202, No. 2013AA050903, No. 2011AA11A257 and No. 2011AA11A254), the Tsinghua University Initiative Scientific Research Program (Grant No. 2010THZ08116, No. 2011THZ08139, No. 2011THZ01004 and No. 2012THZ08129) and State Key Laboratory of Automotive Safety and Energy (No. ZZ2012-011), Suzhou (Wujiang) Automotive Research Institute (Project No.2012WJ-A-01).

Notes and references

1. A. K. Padhi, K. S. Nanjundaswamy and J. B. Goodenough, *Journal of The Electrochemical Society*, 1997, **144**, 1188-1194.
2. Z. Y. Bi, X. D. Zhang, W. He, D. D. Min and W. S. Zhang, *RSC Adv.*, 2013, **3**, 19744-19751.
3. L. Dimesso, C. Forster, W. Jaegermann, J. P. Khanderi, H. Tempel, A. Popp, J. Engstler, J. J. Schneider, A. Sarapulova, D. Mikhailova, L. A. Schmitt, S. Oswald and H. Ehrenberg, *Chem. Soc. Rev.*, 2012, **41**, 5068-5080.
4. Y. Gu, X. Zhang, S. Lu, T. Zhao and D. Jiang, *Chinese Journal of Power Sources*, 2013, **37**, 147-151.
5. L. X. Yuan, Z. H. Wang, W. X. Zhang, X. L. Hu, J. T. Chen, Y. H. Huang and J. B. Goodenough, *Energy Environ. Sci.*, 2011, **4**, 269-284.
6. Y. Zhang, Q. Y. Huo, P. P. Du, L. Z. Wang, A. Q. Zhang, Y. H. Song, Y. Lv and G. Y. Li, *Synth. Met.*, 2012, **162**, 1315-1326.
7. C. Ouyang, S. Shi, Z. Wang, X. Huang and L. Chen, *Physical Review B*, 2004, **69**, 104303.
8. G. Wang, X. Shen and J. Yao, *Journal of Power Sources*, 2009, **189**, 543-546.
9. M. S. Islam, D. J. Driscoll, C. A. J. Fisher and P. R. Slater, *Chemistry of Materials*, 2005, **17**, 5085-5092.
10. S. L. Bewlay, K. Konstantinov, G. X. Wang, S. X. Dou and H. K. Liu, *Materials Letters*, 2004, **58**, 1788-1791.
11. F. Y. Kang, J. Ma and B. H. Li, *New Carbon Mater.*, 2011, **26**, 161-170.
12. R. Orinakova, A. Fedorkova and A. Orinak, *Chem. Pap.*, 2013, **67**, 860-875.

13. K. L. Harrison, C. A. Bridges, M. P. Paranthaman, C. U. Segre, J. Katsoudas, V. A. Maroni, J. C. Idrobo, J. B. Goodenough and A. Manthiram, *Chemistry of Materials*, 2013, **25**, 768-781.
14. S. B. P. Chang Kyoo Park, Ho Chul Shin, Won Il Cho, and Ho Jang, *Bulletin of the Korean Chemical Society*, 2011, **32**, 5.
15. M. Wagemaker, B. L. Ellis, D. Lützenkirchen-Hecht, F. M. Mulder and L. F. Nazar, *Chemistry of Materials*, 2008, **20**, 6313-6315.
16. Z. Ma, G. Shao, Y. Fan, G. Wang, J. Song and T. Liu, *ACS Applied Materials & Interfaces*, 2014, **6**, 9236-9244.
17. C. Nan, J. Lu, L. Li, L. Li, Q. Peng and Y. Li, *Nano Res.*, 2013, **6**, 469-477.
18. B. J. Paul, S.-W. Kang, J. Gim, J. Song, S. Kim, V. Mathew and J. Kim, *Journal of The Electrochemical Society*, 2014, **161**, A1468-A1473.
19. A. V. Murugan, T. Muraliganth, P. J. Ferreira and A. Manthiram, *Inorganic Chemistry*, 2009, **48**, 946-952.
20. C. Sun, S. Rajasekhara, J. B. Goodenough and F. Zhou, *Journal of the American Chemical Society*, 2011, **133**, 2132-2135.
21. B. Ellis, W. H. Kan, W. R. M. Makahnouk and L. F. Nazar, *Journal of Materials Chemistry*, 2007, **17**, 3248-3254.
22. L. Wang, X. He, W. Sun, J. Wang, Y. Li and S. Fan, *Nano Letters*, 2012, **12**, 5632-5636.
23. S. Lemmer and F. Ruether, *Chemical Engineering Science*, 2012, **77**, 143-149.
24. W. Kang, C. Zhao, R. Liu, F. Xu and Q. Shen, *CrystEngComm*, 2012, **14**, 2245-2250.
25. J. Chen and M. S. Whittingham, *Electrochemistry Communications*, 2006, **8**, 855-858.
26. X. Qin, X. Wang, H. Xiang, J. Xie, J. Li and Y. Zhou, *The Journal of Physical Chemistry C*, 2010, **114**, 16806-16812.
27. J. Ni, M. Morishita, Y. Kawabe, M. Watada, N. Takeichi and T. Sakai, *Journal of Power Sources*, 2010, **195**, 2877-2882.
28. C. Nan, J. Lu, C. Chen, Q. Peng and Y. Li, *Journal of Materials Chemistry*, 2011, **21**, 9994-9996.
29. J. Lim, J. Gim, S.-W. Kang, S. Baek, H. Jeong and J. Kim, *Journal of The Electrochemical Society*, 2012, **159**, A479-A484.
30. M. K. Devaraju and I. Honma, *Advanced Energy Materials*, 2012, **2**, 284-297.
31. K. Kanamura, S. Koizumi and K. Dokko, *J Mater Sci*, 2008, **43**, 2138-2142.
32. J. Liu, R. Jiang, X. Wang, T. Huang and A. Yu, *Journal of Power Sources*, 2009, **194**, 536-540.
33. K. Dokko, S. Koizumi, H. Nakano and K. Kanamura, *Journal of Materials Chemistry*, 2007, **17**, 4803-4810.
34. J. Lee and A. S. Teja, *The Journal of Supercritical Fluids*, 2005, **35**, 83-90.

35. F. Iskandar, A. S. Nisa and M. M. Munir, Rural Information & Communication Technology and Electric-Vehicle Technology (rICT & ICeV-T), 2013 Joint International Conference on, 2013.
36. T. Muraliganth, A. V. Murugan and A. Manthiram, *Journal of Materials Chemistry*, 2008, **18**, 5661-5668.
37. Z. Dai, L. Wang, F. Ye, C. Huang, J. Wang, X. Huang, J. Wang, G. Tian, X. He and M. Ouyang, *Electrochimica Acta*, 2014, **134**, 13-17.
38. K. Saravanan, P. Balaya, M. V. Reddy, B. V. R. Chowdari and J. J. Vittal, *Energy Environ. Sci.*, 2010, **3**, 457-463.
39. Y. Wang, J. Wang, J. Yang and Y. Nuli, *Adv. Funct. Mater.*, 2006, **16**, 2135-2140.
40. A. Yamada, S. C. Chung and K. Hinokuma *Journal of The Electrochemical Society*, 2001, **148**, A224-A229.
41. S. Lim, C. S. Yoon and J. Cho, *Chemistry of Materials*, 2008, **20**, 4560-4564.
42. P. Axmann, C. Stinner, M. Wohlfahrt-Mehrens, A. Mauger, F. Gendron and C. M. Julien, *Chemistry of Materials*, 2009, **21**, 1636-1644.
43. C. Delacourt, P. Poizot, J.-M. Tarascon and C. Masquelier, *Nat Mater*, 2005, **4**, 254-260.
44. Y. Wang, Z.-s. Feng, J. Hu, L. Yu, J.-j. Chen, L.-l. Wang, X.-j. Wang and H.-l. Tang, *Electrochimica Acta*, 2014, **117**, 431-437.
45. J. Chen and J. Graetz, *ACS Applied Materials & Interfaces*, 2011, **3**, 1380-1384.
46. M.-H. Lee, T.-H. Kim, Y. S. Kim and H.-K. Song, *The Journal of Physical Chemistry C*, 2011, **115**, 12255-12259.
47. X. Sun and Y. Xu, *Materials Letters*, 2012, **84**, 139-142.
48. G. Meligrana, C. Gerbaldi, A. Tuel, S. Bodoardo and N. Penazzi, *Journal of Power Sources*, 2006, **160**, 516-522.
49. D. Y. W. Yu, K. Donoue, T. Kadohata, T. Murata, S. Matsuta and S. Fujitani, *Journal of The Electrochemical Society*, 2008, **155**, A526-A530.
50. U. Holzwarth and N. Gibson, *Nat Nano*, 2011, **6**, 534-534.
51. H. Borchert, E. V. Shevchenko, A. Robert, I. Mekis, A. Kornowski, G. Grübel and H. Weller, *Langmuir*, 2005, **21**, 1931-1936.
52. D.-H. Kim and J. Kim, *Electrochemical and Solid-State Letters*, 2006, **9**, A439-A442.
53. L. Wang, G. Liang, X. Ou, X. Zhi, J. Zhang and J. Cui, *Journal of Power sources*, 2009, **189**, 423-428.
54. T. Azib, S. Ammar, S. Nowak, S. Lau-Truing, H. Groult, K. Zaghib, A. Mauger and C. Julien, *Journal of Power Sources*, 2012, **217**, 220-228.
55. L. Wang, F. Zhou, Y. S. Meng and G. Ceder, *Physical Review B*, 2007, **76**, 165435.
56. K. A. Persson, B. Waldwick, P. Lazic and G. Ceder, *Physical Review B*, 2012, **85**, 235438.

57. K. Dokko, S. Koizumi and K. Kanamura, *Chemistry Letters*, 2006, **35**, 338-339.

Figure captions:

Fig. 1 SEM images of (a) S1, rectangular nanoplates; (b) S2, rectangular nanoplates; (c) S3, long hexagon nanorods; (d) S4, long hexagon nanorods; (e) S5, spindle plates; (f) S6, spindle plates.

Fig. 2 TEM(left), HRTEM(middle) and their corresponding FFT (right)images of (a) S1, rectangular nanoplates (exposed (100) face); (b) S3, long hexagon nanorods: (b-1) long hexagon shape shows the exposed (010) face, (b-2) rectangular shape shows the exposed (100) face; (c) S5, spindle plates shown the predominant face (010).

Fig. 3 XRD patterns of the six $LiFePO_4$ crystals (S1~S6) obtained via solvothermal treatment. S1~S4 are well indexed to olivine $LiFePO_4$ patterns, while S5 and S6 samples show obvious impurity Fe_3O_4 patterns.

Fig. 4 The particle morphology evolution with the acidity (pH) of solvothermal synthesis environment. Rectangular nanoplates with main exposed (100) face transfer to spindle plates predominantly exposed (010) face gradually as pH of mother solutions increases from 2.56 to 5.80.

Fig. 5 Schematic illustration of pH influences on $LiFePO_4$ solvothermal process. *i* is isoelectric point which refers to a certain pH value during the solvothermal process. when the solution pH<*i*, the net residual electric charge on the surface of the $LiFePO_4$ particles is expected to be positive, and faces attract different kinds of OH^-, SO_4^{2-}, $HO\text{-}CH_2\text{-}CH_2\text{-}O^-$ or $^-O\text{-}CH_2\text{-}CH_2\text{-}O^-$ negative ions and complexes; when pH>*i*, the particle surface is negatively charged. Particle surfaces will be capped by EG molecules and cations.

Fig. 6 Comparison of the specific discharge capacities of the carbon coated $LiFePO_4$ particles prepared via solvothermal method at different primary $LiOH/H_3PO_4$ mole ratios. S3 and S4 show the best rate performances with about 130 mAh g^{-1} specific discharge capacity at 10C at $LiOH/H_3PO_4$=2.7~3.0. S5 and S6 show the worst performances for about 70 mAh g^{-1} at 0.1C.

Fig. 7 The first cycle discharge curves of carbon coated $LiFePO_4$ synthesized at $LiOH/H_3PO_4$=3.0 at different C rates: 169.9, 155.8, 147.0, 145.5, 143.1, 138.5 and 129.8 mAh g^{-1} at 0.1C, 0.2C, 0.5C, 1C, 2C, 5C and 10C individually.

Fig. 8 Comparison of XRD patterns of different $LiFePO_4$ samples annealed at 650˚C for 5 hours: (a) without carbon coated; (b) with carbon coated. After high temperature treatment, Li_3PO_4 and Fe_3O_4 impurities are indexed for samples S3-a and S5-a without carbon coating. Impurities disappear when carbon is coated on sample S3 surface. The impurities' relative intensity decreased for all samples coated by carbon. $Fe_3Fe_4(PO_4)_6$ is also indexed in XRD patterns of carbon coated sample S5-c.

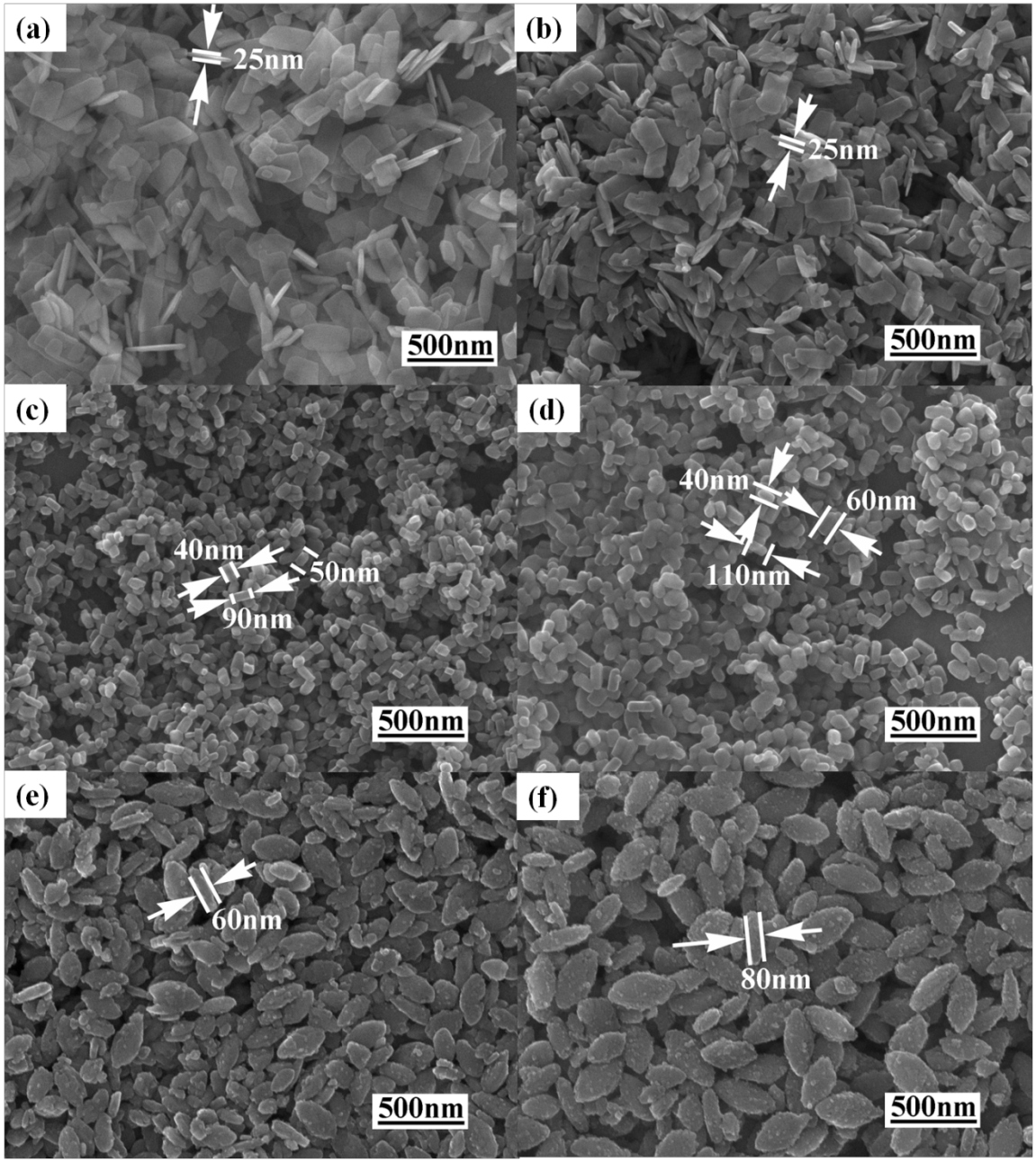

Fig. 1 SEM images of (a) S1, rectangular nanoplates; (b) S2, rectangular nanoplates; (c) S3, long hexagon nanorods; (d) S4, long hexagon nanorods; (e) S5, spindle plates; (f) S6, spindle plates.

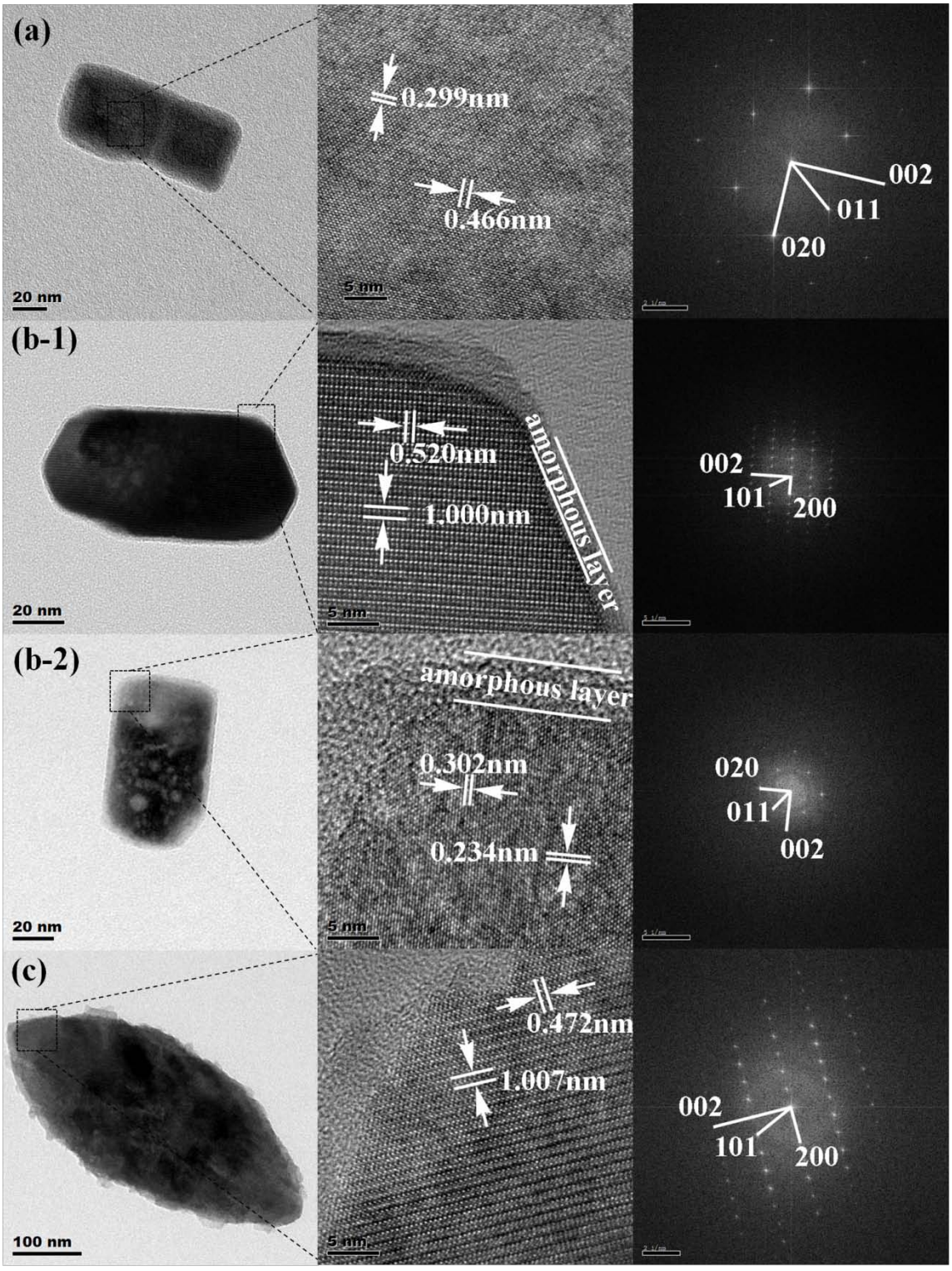

Fig. 2 TEM(left), HRTEM(middle) and their corresponding FFT (right)images of (a) S1, rectangular nanoplates (exposed (100) face); (b) S3, long hexagon nanorods: (b-1) long hexagon shape shows the exposed (010) face, (b-2) rectangular shape shows the exposed (100) face; (c) S5, spindle plates shown the predominant face (010).

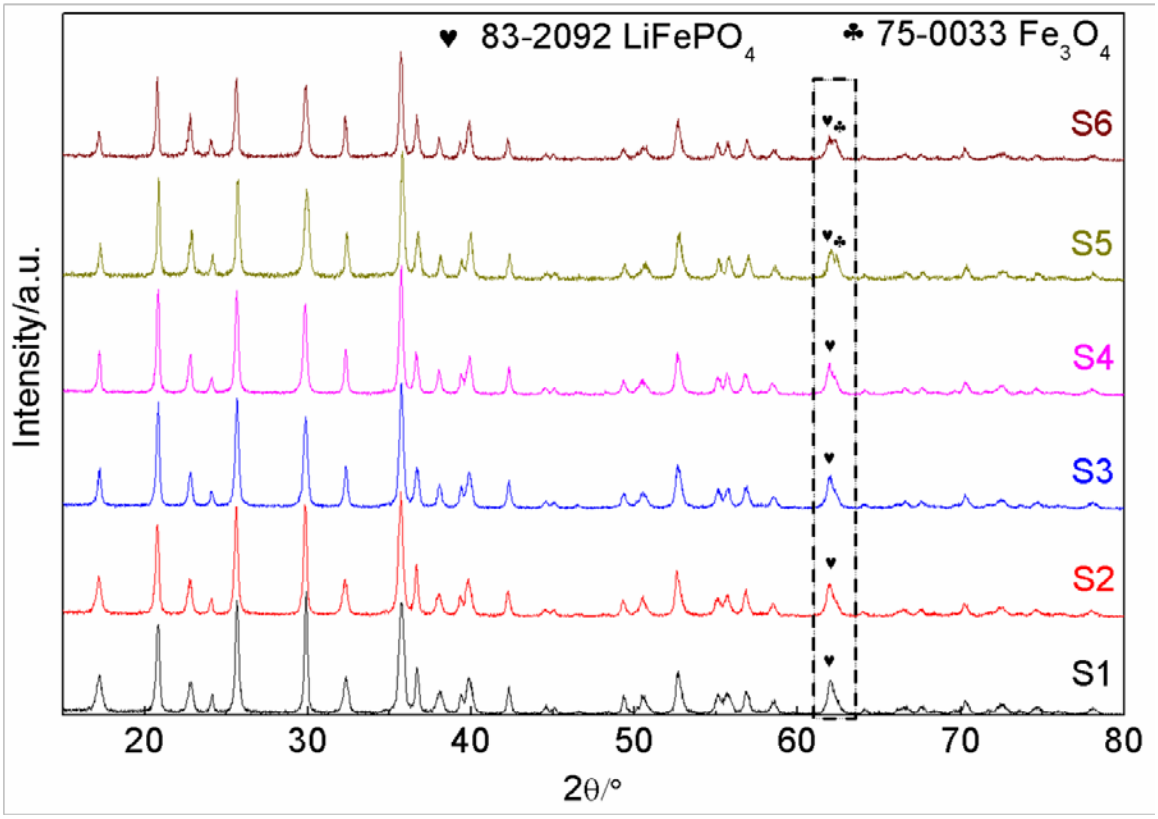

Fig. 3 XRD patterns of the six $LiFePO_4$ crystals (S1~S6) obtained via solvothermal treatment. S1~S4 are well indexed to olivine $LiFePO_4$ patterns, while S5 and S6 samples show obvious impurity Fe_3O_4 patterns.

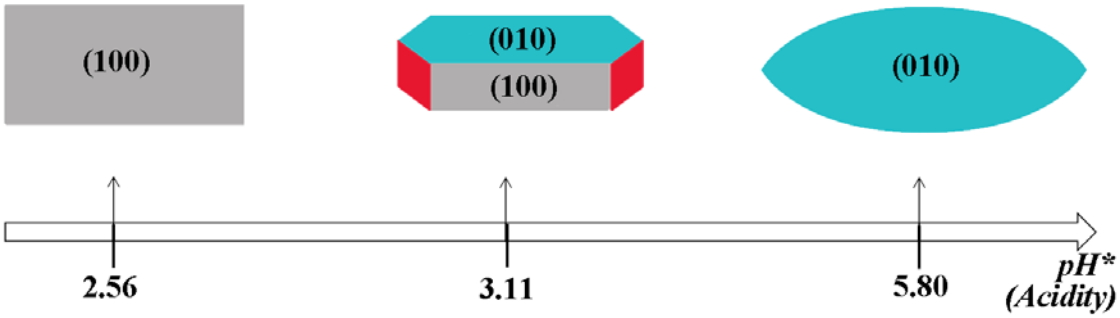

Fig. 4 The particle morphology evolution with the acidity (pH) of solvothermal synthesis environment. Rectangular nanoplates with main exposed (100) face transfer to spindle plates predominantly exposed (010) face gradually as pH of mother solutions increases from 2.56 to 5.80.

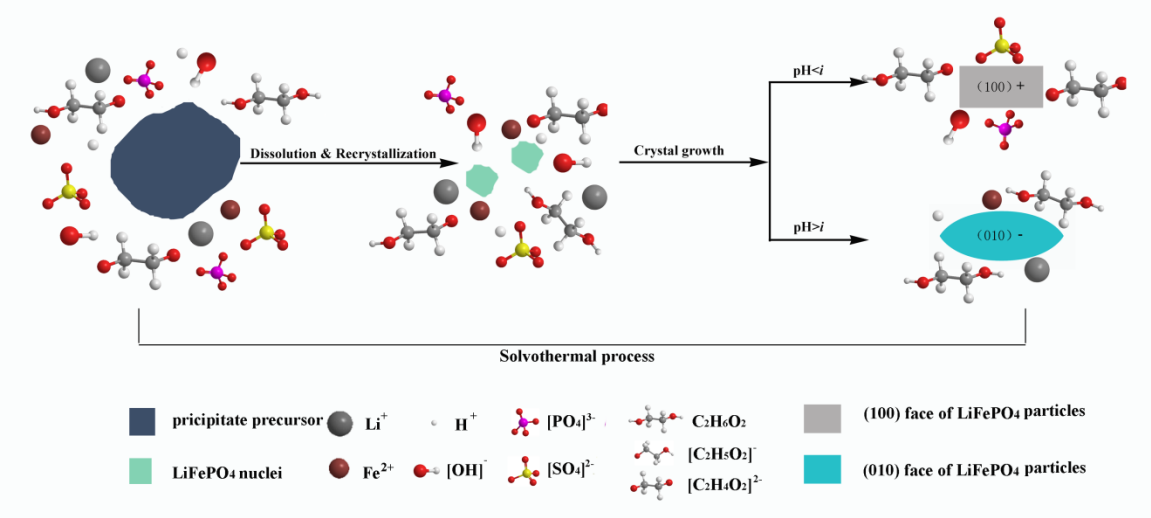

Fig. 5 Schematic illustration of pH influences on $LiFePO_4$ solvothermal process. *i* is isoelectric point which refers to a certain pH value during the solvothermal process. when the solution pH<*i*, the net residual electric charge on the surface of the $LiFePO_4$ particles is expected to be positive, and faces attract different kinds of OH^-, SO_4^{2-}, $HO\text{-}CH_2\text{-}CH_2\text{-}O^-$ or $^-O\text{-}CH_2\text{-}CH_2\text{-}O^-$ negative ions and complexes; when pH>*i*, the particle surface is negatively charged. Particle surfaces will be capped by EG molecules and cations.

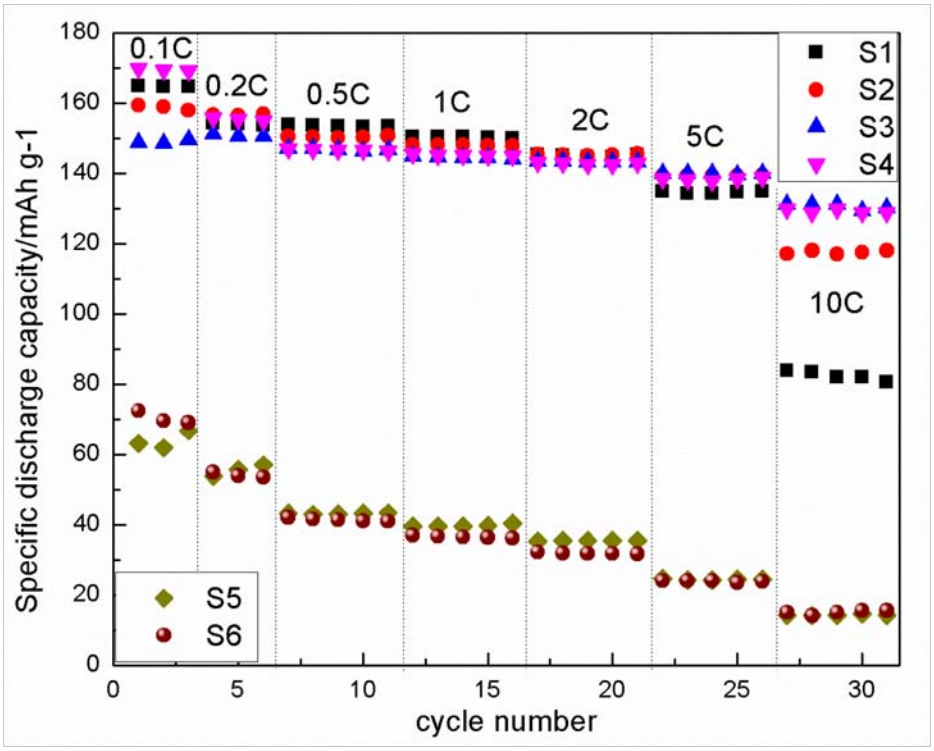

Fig. 6 Comparison of the specific discharge capacities of the carbon coated $LiFePO_4$ particles prepared via solvothermal method at different primary $LiOH/H_3PO_4$ mole ratios. S3 and S4 show the best rate performances with about 130 mAh g^{-1} specific discharge capacity at 10C at $LiOH/H_3PO_4$=2.7~3.0. S5 and S6 show the worst performances for about 70 mAh g^{-1} at 0.1C.

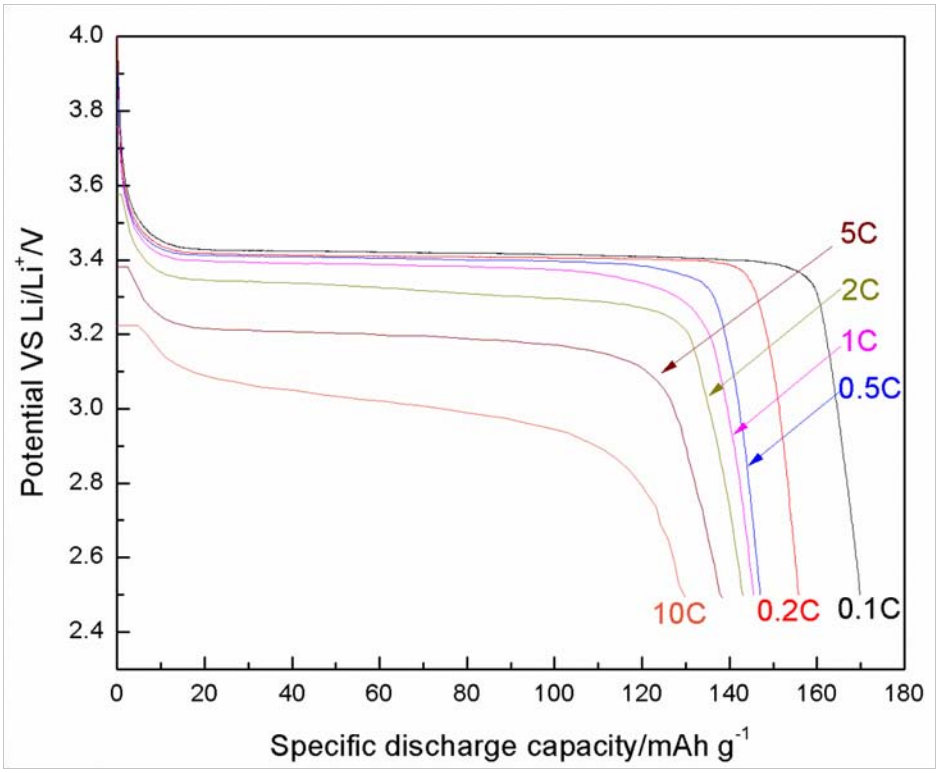

Fig. 7 The first cycle discharge curves of carbon coated $LiFePO_4$ synthesized at $LiOH/H_3PO_4$=3.0 at different C rates: 169.9, 155.8, 147.0, 145.5, 143.1, 138.5 and 129.8 mAh g^{-1} at 0.1C, 0.2C, 0.5C, 1C, 2C, 5C and 10C individually.

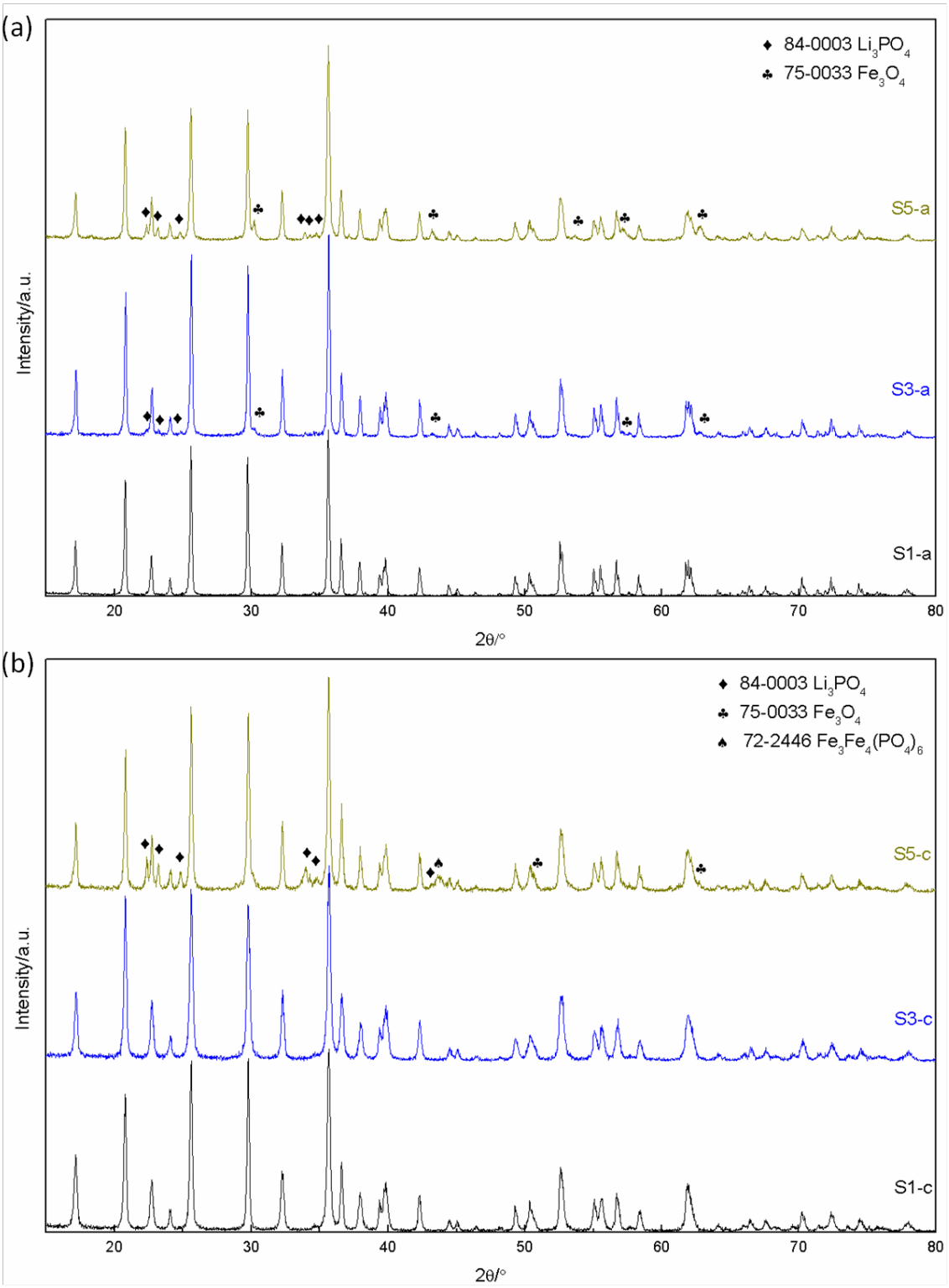

Fig. 8 Comparison of XRD patterns of different $LiFePO_4$ samples annealed at 650˚C for 5 hours: (a) without carbon coated; (b) with carbon coated. After high temperature treatment, Li_3PO_4 and Fe_3O_4 impurities are indexed for samples S3-a and S5-a without carbon coating. Impurities disappear when carbon is coated on sample S3 surface. The impurities' relative intensity decreased for all samples coated by carbon. $Fe_3Fe_4(PO_4)_6$ is also indexed in XRD patterns of carbon coated sample S5-c.

Table of Contents

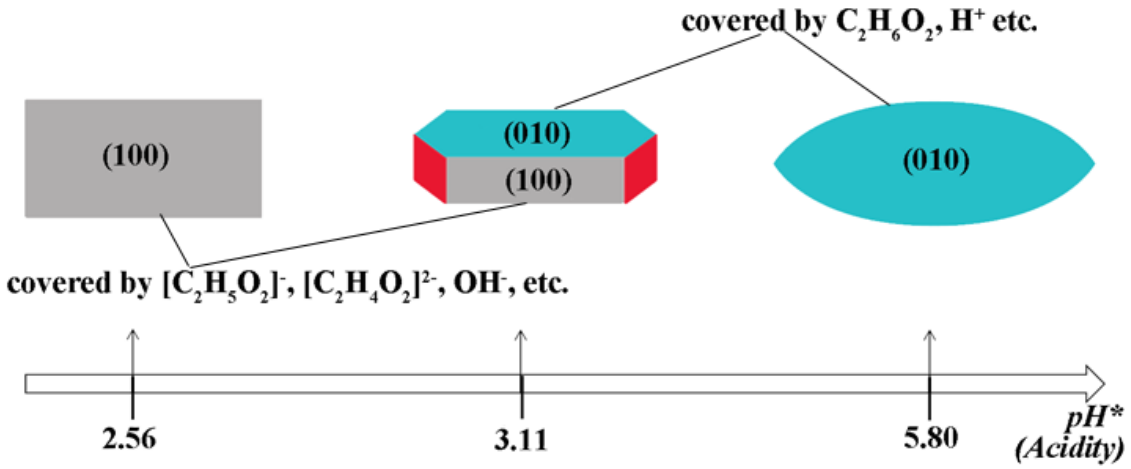

LiFePO4 crystal orientation varies from (100) to (010) due to different species covering with pH increase during solvothermal synthesis.